Iranian Journal of Basic Medical Sciences
ijbms.mums.ac.ir

Modulation of CCL5 and CXCR4 as EMT signaling biomarkers by cold atmospheric plasma and Anti-PD-1 combination therapy in melanoma: Insights from integrated bioinformatics and *in vitro* and *in vivo* validation

Zeinab Rostami [1, 2], Fatemeh Akhoundi [3], Zahra Yazdani [1, 2], Mohammad Eslamijouybari [4], Mansooreh Mirzaei [5], Forouzan Bousaeedi [1, 2], Ghazaleh Rostami [2], Alireza Rafiei [1*]

[1] Department of Immunology, School of Medicine, Mazandaran University of Medical Sciences, Sari, Iran
[2] Student Research Committee, School of Medicine, Mazandaran University of Medical Sciences, Sari, Iran
[3] Department of Genetics, Faculty of Basic Sciences, Shahrekord University, Shahrekord, Iran
[4] Gastrointestinal Cancer Research Center, Non-Communicable Diseases Institute, Mazandaran University of Medical Sciences, Sari, Iran
[5] Department of Anatomy, School of Medicine, Mazandaran University of Medical Sciences, Sari, Iran

ARTICLE INFO

Article type:
Original

Article history:
Received: Sep 19, 2025
Accepted: Feb 22, 2026

Keywords:
Anti-PD-1
C-X-C chemokine receptor - type 4 (CXCR4)
C-C motif chemokine ligand - 5 (CCL5)
Cold atmospheric plasma - (CAP)
Epithelial-mesenchymal - transition (EMT)
Melanoma

ABSTRACT

Objective(s): Cold atmospheric plasma (CAP) has emerged as a promising non-thermal modality with anticancer effects. Combining CAP with immune checkpoint blockade (ICB) may enhance therapeutic efficacy, yet the molecular targets underlying this synergy remain incompletely understood.

Materials and Methods: Epithelial–mesenchymal transition (EMT)–associated genes responsive to CAP and Anti-PD-1 therapy were identified by integrating bioinformatics analyses of melanoma transcriptomic data with *in vitro* and *in vivo* experiments. Weighted gene co-expression network analysis (WGCNA), GO, and KEGG enrichment identified key modules and candidate genes. The effects of CAP, Anti-PD-1, and their combination on cell viability and gene expression were evaluated in B16F10 melanoma cells, L929 fibroblasts, and a syngeneic mouse melanoma model.

Results: WGCNA highlighted CCL5 and CXCR4 as hub genes enriched in EMT-related pathways. MTT assays showed that CAP reduced B16F10 cell viability, an effect further enhanced by Anti-PD-1, while sparing L929 fibroblasts. In tumor-bearing mice, combination therapy produced the most pronounced tumor regression and down-regulation of CCL5 and CXCR4 compared with single treatments. Minimal viability or expression changes were observed in normal fibroblasts or untreated controls.

Conclusion: CAP and Anti-PD-1 combination therapy effectively suppressed melanoma cell viability and modulated EMT-associated gene expression both *in vitro* and *in vivo*. We further explored a potential molecular mechanism underlying this therapeutic effect, revealing that the EMT-related genes CCL5 and CXCR4 play a vital role in this response. These findings highlight the relevance of these pathways and support the potential of combining CAP with ICB as a promising approach for melanoma treatment.

▶ Please cite this article as:
Rostami Z, Akhoundi F, Yazdani Z, Eslamijouybari M, Mirzaei M, Bousaeedi F, Rostami Gh, Rafiei AR. AModulation of CCL5 and CXCR4 as EMT signaling biomarkers by cold atmospheric plasma and Anti-PD-1 combination therapy in melanoma: Insights from integrated bioinformatics and *in vitro* and *in vivo* validation. Iran J Basic Med Sci 2026; 29: 1052-1065. doi: https://dx.doi.org/10.22038/ijbms.2026.91340.19707

Introduction

Over the past three decades, cutaneous melanoma has steadily increased worldwide (1). Melanoma is a highly aggressive and resistant type of skin cancer, representing only 1% of all skin cancers but accounting for the majority of skin cancer-related deaths. The 5-year survival rate for primary melanoma is impressive at 99%; however, this figure plummets to just 27% for metastatic melanoma, underscoring the critical importance of early diagnosis and treatment for improving prognosis and survival (2, 3). Therapies for melanoma comprise traditional chemotherapy (dacarbazine) (4), a combination of chemotherapy with interleukin-2 and interferon-α (5), targeted treatments using small molecules for mutated BRAF (6), and ICB (Anti-CTLA4 and Anti-PD-1) (7). Despite advancements in treatment methods, the variability present in tumors leads to differing levels of resistance and survival, which ultimately limits disease-free survival for patients (8).

Checkpoint inhibitor molecules have emerged as effective therapies for melanoma (9, 10). Among these therapies, Anti-PD-1 is commonly used, as it binds to Programmed Cell Death Protein 1 (PD-1) receptors on the surfaces of both cancer and immune cells, thereby inhibiting tumor growth while simultaneously boosting immune cell activity (11, 12). However, the potential for serious side effects necessitates a cautious application of these therapies, underscoring the urgent need for new combination strategies (12).

Recently, CAP devices operating at room temperature

*Corresponding author: Alireza Rafiei. Department of Immunology, School of Medicine, KM 18, Khazarabad Road, Khazar Square, Sari, Iran. Email: rafiei1710@gmail.com

and atmospheric pressure have shown significant promise for biomedical uses, including cancer therapy (13, 14). CAP is a weakly ionized gas (typically <1% ionization). Plasma is often referred to as the fourth state of matter and consists of a complex mixture of electrons, ions, neutral particles, reactive oxygen and nitrogen species (RONS), electromagnetic fields, and ultraviolet (UV) radiation, all of which may contribute to its biological effects (15). The anticancer activity of CAP has been shown to largely depend on the combined action of RONS on the target tissue (16).

The most significant aspect is likely the selective impact of CAP on normal and cancer cells, which in turn results in a decrease in the side effects of this approach compared to traditional methods. Tumor cells often maintain elevated basal RONS levels, which makes them more vulnerable to additional oxidative stress from CAP compared to many normal cells. Nonetheless, the effectiveness of CAP is inadequate due to its limited penetration into tumor tissues, necessitating multiple and repeated CAP treatments to achieve optimal results (13, 15).

CAP has been reported to release tumor-related antigens and may enhance the maturation of dendritic cells (DCs) in tumor-draining lymph nodes. Mature DCs present tumor-derived peptides via major histocompatibility complexes to T cells, initiating anti-tumor immune responses (17). These responses could be further augmented by immune checkpoint inhibitors such as Anti-PD-1 antibodies. In addition, CAP has been observed to down-regulate PD-1/PD-L1 expression in tumor cells (18, 19). Supporting this notion, Chen *et al* (2020) demonstrated that combining CAP with Anti-PD-L1 therapy *in vivo* enhanced anti-tumor immunity, highlighting the potential of CAP to synergize with checkpoint blockade in cancer therapy (20).

CAP application has been shown to diminish EMT in melanoma cells (21). PD-1 proteins present on cancer cell surfaces have been suggested to enhance the EMT process and tumor advancement, suggesting that using a PD-1 antagonist could potentially reduce the EMT process in cancer cells (22, 23). EMT is a crucial mechanism in tumor invasion and metastasis, and contributes to drug resistance (24). During the EMT process, epithelial cells shed their distinctive traits and acquire mesenchymal cell characteristics, such as invasiveness and the ability to migrate (25).

Presently, the tumor-node-metastasis (TNM) staging system remains a widely used approach for predicting the clinical prognosis of patients with melanoma. However, due to the considerable heterogeneity of melanoma, patients with the same TNM stage who receive identical treatment modalities often experience a range of clinical outcomes (26). As a result, developing novel and effective gene signatures is essential for more precise patient stratification, which can ultimately improve the prognosis for melanoma patients. Currently, gene signatures, including long non-coding RNAs and mRNAs, are gaining importance in melanoma prognosis (27, 28).

This research identified a novel signature based on EMT-related gene sets that effectively predict outcomes for melanoma cases. To achieve this, original sample data from Recount, and Gene Expression Omnibus (GEO) databases were downloaded. Bioinformatics methods were used to select and evaluate hub genes associated with the EMT pathway as significant prognostic markers in melanoma. This evaluation was performed both before and after treatment of melanoma cells (B16F10), normal fibroblasts (L929), and tumor-bearing mice with CAP, Anti-PD-1, or their combination. The overall experimental workflow, including both *in vitro* and *in vivo* phases, is illustrated in (Figure 1). The findings have the potential to enhance our understanding of these therapeutic approaches and represent a significant advancement toward improved treatment options for melanoma.

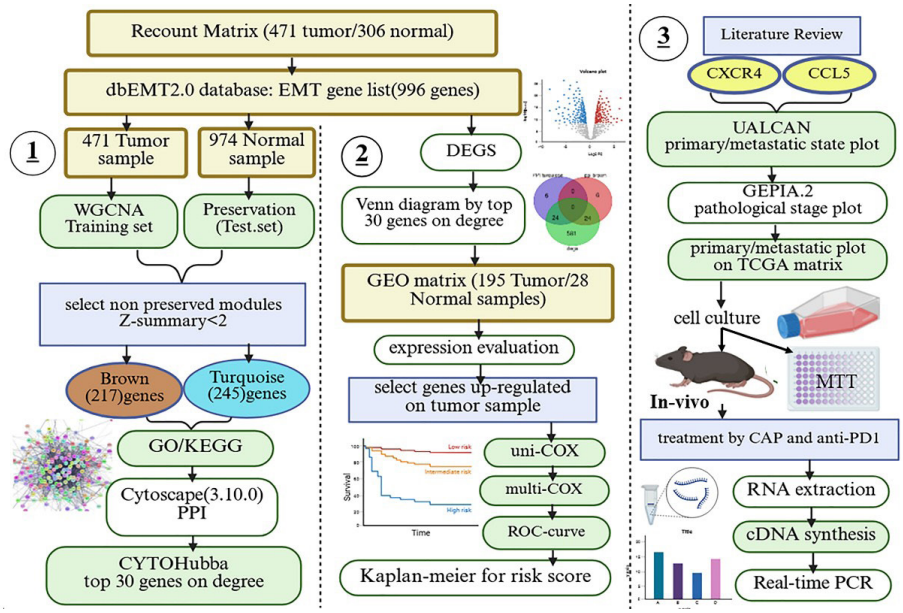

Figure 1. Flowchart depicting the steps of data preparation, processing, analysis, and validation in this study

The analysis integrates multiple datasets, including Recount and GEO, alongside EMT gene lists. WGCNA module selection was conducted on tumor samples, and module preservation was assessed on normal samples. Key steps involved pathway enrichment (GO/KEGG), PPI analysis, and COX regression to identify significant genes (CXCR4 and CCL5). These genes were further analyzed using primary/metastatic state plots and pathological stage plots. Experimental validation included gene expression evaluation in melanoma cell culture under treatment with CAP and Anti-PD-1, followed by RNA extraction, cDNA synthesis, and Real-time PCR, as well as in vivo assessment of tumor tissues from treated tumor-bearing mice.

GEO: Gene expression omnibus, EMT: Epithelial-mesenchymal transition, WGCNA: Weighted gene co-expression network analysis, GO: Gene ontology, KEGG: Kyoto encyclopedia of genes and genomes, PPI: Protein-protein interaction, CAP: Cold atmospheric plasma

Table 1. Summary of the cancer genome atlas (TCGA) RNA-seq datasets used in this study

Source	Sample type	Initial count	Filtering/Selection	Final count used	Notes
TCGA-SKCM	Tumor	471	None	471	Labeled as sample type "01"
	Normal	1	Removed	0	Labeled as sample type "14", excluded for consistency
Recount project	Normal skin tissue	974	PCA clustering → selected one cluster	306	Chose cluster most distinct from TCGA tumors
total used				777	471 tumors + 306 normals

Note: TCGA and Recount datasets were merged after log-transformation and preprocessed using the TCGAbiolinks R package. PCA was performed on Recount data to reduce batch effects and ensure comparability with TCGA tumor samples.

Materials and Methods

Data retrieval and data preprocessing

An RNA-sequencing dataset comprising 471 tumor samples and one normal sample from Skin Cutaneous Melanoma (SKCM) was obtained from The Cancer Genome Atlas (TCGA). A total of 974 normal skin tissue RNA-seq samples were retrieved from the Recount database (https://jhubiostatistics.shinyapps.io/recount/), which provides uniformly processed RNA-seq data from public studies. Principal Component Analysis (PCA) was applied to the Recount dataset, revealing two distinct clusters. From these, a well-separated cluster of 306 samples was selected to ensure comparability with the TCGA tumor cohort. The single normal sample originally present in the TCGA dataset (barcode type "14") was excluded to maintain consistency in the normal group.

Following this selection, the final dataset used for downstream analyses included 471 tumor samples from TCGA and 306 normal skin samples from Recount (total N = 777). Gene expression data were log2-transformed, and the samples were merged and processed using the TCGAbiolinks R package (Table 1) (29-31). The corresponding clinical and prognostic parameters were also obtained from TCGA through https://jhubiostatistics.shinyapps.io/recount/ (32) (Supplementary Table 1).

Additionally, gene expression profiles from 195 patients and 28 normal samples with SKCM were downloaded from GEO: GSE15605, GSE46517, and GSE7553 cohort (https://www.ncbi.nlm.nih.gov/geo/) as a validation cohort (Table 2) (33). To integrate gene expression data across different microarray platforms (GPL570 for GSE15605 and GSE7553; GPL96 for GSE46517), Gene-level mapping was performed to retain only common genes, followed by batch effect correction using the ComBat algorithm (sva package).

Identification of EMT states and EMT-related DEGs

To effectively manage a large number of genes, Gene filtering was conducted using the EMT pathway genes obtained from the dbEMT2.0 database (https://dbemt.bioinfo-minzhao.org/index. html). A total of 1,184 EMT-related hallmark genes were extracted from this database, including 1,011 protein-coding genes and 173 non-coding RNAs. These genes were extracted from the expression matrix. All gene profiles from different platforms were normalized using the R package "sva" to remove batch effects identified in previous studies (34, 35). After preparing the data, we used the R package Limma to obtain differential gene expression (DGE) between normal and tumor samples in the Recount matrix (36, 37).

Co-expression network construction

WGCNA was employed as a bioinformatics approach to construct gene expression patterns from multiple samples. This method generated clusters of genes with similar expression profiles based on Pearson correlation, enabling analysis of the relationships between these clusters (modules) and specific traits or phenotypes (38). First, normal data were separated from the 471 tumor samples, after which the WGCNA was initiated.

Six co-expressed modules were identified, ranging in size from 34 to 241 genes, each assigned a specific color for reference. The "grey" module was designated for genes that were not co-expressed. The genes in each module were listed in (Supplementary Table 2). First, the optimal soft threshold was determined based on the mean connectivity and scale independence values. Next, the correlation values between pairs of genes were calculated exponentially using this soft threshold, and the results were organized into clusters. Finally, the correlation was calculated between the principal components of gene modules and the clinical features.

Module preservation analysis

In this analysis, the normal Recount data were used as the test set and the tumor data as the training set. If the Z-summary was below 2, it was considered that the module was not preserved. A Z-summary between 2 and 10 was regarded as moderate preservation, whereas a Z-summary above 10 indicated strong preservation. Modules that were not preserved were of interest in this study; therefore, those with a Z-summary of 2 or lower were selected. Additionally, a median rank exceeding the threshold of 5.5 was considered indicative of better preservation.

Gene ontology (GO) and pathway enrichment analysis

GO analysis was employed as a valuable method for annotating genes and gene sets with their biological characteristics, particularly when high-throughput genome or transcriptome data were analyzed (39). The Kyoto

Table 2. Gene expression datasets from gene expression omnibus (GEO) used in this study

Dataset	Platform (GPL)	Tumor samples	Normal samples	Total samples
GSE15605	GPL570 (Affymetrix Human Genome U133 Plus 2.0)	58	16	74
GSE46517	GPL96 (Affymetrix Human Genome U133A)	83	8	111
GSE7553	GPL570 (Affymetrix Human Genome U133A)	54	4	58

Encyclopedia of Genes and Genomes (KEGG) pathway serves as a knowledge base for the systematic analysis of gene functions (40). In this study, GO and KEGG pathway enrichment analyses were performed for the brown and turquoise modules using the ClusterProfiler R package, which provides a comprehensive set of functions for statistical analysis and visualization of functional profiles for genes and gene clusters. A false discovery rate (FDR) of less than 0.05 was used as the cut-off criterion for significance in both analyses.

PPI Network and hub genes selection

Protein-protein interaction (PPI) networks offer insights into the molecular mechanisms that underlie cellular activities. In this study, a PPI network was constructed focusing on the brown and turquoise modules using the Search Tool for the Retrieval of Interacting Genes (STRING) database. STRING, version 9.0, supports data from 1,133 organisms and includes information on 5,214,234 proteins (41). The Cytoscape program (version 3.10.0) was used to visualize the PPI network. A confidence score of 0.4 was established as the cutoff criterion, and the top 30 genes in the brown and turquoise modules, based on node degrees, were selected using *CytoHubba*. In the following, create a Venn diagram using the Venny 2.1 web tool (https://bioinfogp.cnb.csic.es/tools/venny/index.html, access date: 16 April 2024) to illustrate the important genes based on the degrees of these modules and the DEG.

Hub gene expression evaluation

To complete the gene analysis and filter for the most relevant genes, multiple GSE datasets related to melanoma were downloaded. After preprocessing the data and conducting a meta-analysis, a new data frame was created containing the selected genes. Then, all gene expression profiles were normalized from different platforms using the R package "sva" to eliminate batch effects identified in previous studies (34, 35). The boxplot was generated to compare gene expression levels between normal and tumor tissues and select the up-regulated genes in tumor samples.

Survival analysis and final hub gene selection

This study assessed survival data for proportional hazards and the linearity of quantitative predictors, focusing on the assumptions underpinning Cox regression. Subsequently, both univariable and multivariable Cox regression analyses were conducted to estimate hazard ratios (HR) and 95% confidence intervals (CI) for selected EMT-related genes concerning overall survival (OS), utilizing the "survival" and "survminer" R packages. To assess the predictive accuracy of the prognostic models for patients with melanoma, time-dependent receiver operating characteristic (ROC) curves were generated, and the area under the curve (AUC) was calculated and plotted utilizing the R packages "pROC," "survivalROC," and "ggplot2" (33). Kaplan–Meier survival curves were created to compare OS between high and low-risk groups. The differences in OS between these groups were evaluated using the log-rank test, conducted with the "survival" and "survminer" R packages. Among the identified genes, one was selected for further investigation due to its well-documented association with our treatment conditions, CAP, and Anti-PD-1 therapy, as highlighted in previous studies. Additionally, another gene showed significance in the univariabel Cox model but did not maintain its significance in the multivariabel model. This gene was included in the study because of its strong correlation with the expression of the primary selected gene and its potential involvement in the same biological pathway influenced by CAP and Anti-PD-1 therapy. This integrative approach, which combines survival analysis with relevance to biological pathways, enabled us to identify the most pertinent genes for further experimental validation.

Identification of pathological stages and primary/metastatic status

To further explore the relationship between the expression of these two genes and the pathological stages of patients across melanoma TCGA data, box plots were created to visualize complementary gene expression. This analysis was performed using the GEPIA 2.0 tool (42). The UALCAN web server (https://ualcan.path.uab.edu/) was utilized to investigate the correlation between genes and the primary and metastatic states in melanoma cancer (43). ULCAN serves as a significant online platform that analyzes gene expression data from the TCGA across various cancer types. In this study, the correlation between CCL5 and CXCR4 expression in melanoma metastatic and primary samples is calculated using the TCGA expression matrix. the correlation of CCL5 and CXCR4 expression was evaluated between melanoma metastatic samples and primary samples, as well as the Recount in our expression matrix in this study.

Cell culture

B16F10 and L929 cell lines (from the Pasteur Institute in Tehran, Iran) were used to evaluate cytotoxicity and gene expression under treatment conditions. Although the initial bioinformatics analyses were conducted using human datasets, murine models were employed for experimental validation due to the high conservation of key immune and EMT-related signaling pathways, including CCL5/CCR5 and CXCR4/CXCL12, between humans and mice (44). The cells were cultured in Roswell Park Memorial Institute 1640 (RPMI-1640) medium (Attocell, Austria), supplemented with 10% (v/v) fetal bovine serum (FBS), 100 U/ml of penicillin, and 100 µg/ml of streptomycin, under standard culture conditions of 37 °C, CO_2 5%, and 95% humidity.

CAP device and treatment protocol

CAP treatment was performed using a device developed at the School of Physics, University of Mazandaran, Iran. which has been previously described in detail (45-47). Briefly, the system consists of copper wire electrodes, a grounded copper ring electrode, and a Pyrex tube dielectric, with a 7 mm gap between the electrodes. Argon gas with a purity of 99.9999% was used as the plasma feed. Treatments were conducted at 0–25 kV and 9 kHz, with an argon flow rate of 2.5 l/min, and the plasma source was positioned 4.5 cm above the culture plate. The outlet gas temperature during treatments was maintained at 35–40 °C. Direct CAP exposure was applied to cells seeded in multi-well plates for variable durations (30–120 sec). The hydroxyl radical (OH•) was the most abundant ROS generated by this system, accompanied by other ROS/RNS such as O, O_2^+, O_4^+, O_2^-, O^-, O_3, NO, O_2, and H_2O_2.

Metabolic activity and cell viability

The MTT (3-(4,5-dimethylthiazol-2-yl)-2,5-diphenyltetrazolium bromide) assay was employed to assess the cytotoxic effects of various agents on cells by examining their metabolic activity. For this study, a total of 7 × 10^3 B16F10 and L929 cells were cultured per well in a 96-well plate, with three technical replicates for each group, and

allowed to grow for 24 hr before treatment. Each cell line was divided into four groups: group 1 served as the negative control with untreated cells; group 2 was CAP treatment (30 to 120 sec); and group 3 received Anti-PD-1(Zakaria, Sinagene, Iran) (10–250 µg/ml), which was directly added to the cell culture medium. Following the determination of the appropriate treatment doses, combination treatment was administered in which the Anti-PD-1 antibody was first added to the cells, followed by CAP exposure, for comparison against the selected single treatments. Cells were incubated for 48 hr after treatment, the culture medium was discarded, and the cells were washed with Phosphate-Buffered Saline (PBS). Subsequently, 50 µl of MTT solution (5 mg/ml in PBS, Sigma, USA) was added to each well. After a 4-hr incubation period under standard conditions, the formazan crystals were dissolved by adding 150 µl of dimethylsulfoxide (Merck, Darmstadt, Germany) to each well. Absorbance was then measured at 570 nm using a BioTek microplate reader (BioTek, Winooski, VT, USA). All experiments were performed in three independent biological replicates, and each replicate was measured in technical triplicates to ensure reproducibility.

Animal experiment

Four to six-week-old female C57BL6 mice were housed under standard conditions at the Institute of Laboratory Animals of Mazandaran University of Medical Sciences. To grow melanoma tumors, 10^6 B16F10 cells in 100 µl PBS were injected subcutaneously into the right flank of mice. Ten to 15 days after B16F10 tumor cell inoculation, the tumor diameter reached 5 mm. Tumor-bearing mice were randomly divided into four groups, including (a) untreated controls, (b) CAP, (c) Anti-PD-1, and (d) CAP+Anti-PD-1. Anti-PD-1 was injected intravenously at a dose of 15 mg/kg for 3 injections every three days (48). CAP treatment was performed for 5 minutes, three times, with a 5-day interval. The plasma jet nozzle was positioned on top of the tumor mass at a distance of 15 mm from the skin surface and was continuously moved across the tumor surface during treatment (46). For tumor tissue analysis, mice were sacrificed using carbon dioxide (CO_2) inhalation, in accordance with institutional guidelines (49), and the tissue was stored at −70 ◦C until RNA extraction. This was a preliminary pilot study designed to generate proof-of-concept data. A total of three mice per group were used, consistent with common practices in exploratory pilot experiments aimed at reducing animal use while assessing feasibility (50). Animal health and behavior were monitored daily throughout the study for signs of distress, weight loss (>20%), ulceration, or impaired mobility. Any animal meeting humane endpoints was to be excluded and euthanized according to institutional guidelines. Female C57BL/6 mice were used in this pilot study to minimize biological variability and stress-related confounding factors, consistent with commonly used B16F10 melanoma models (51).

RNA quantification

Total RNA was extracted from 1 × 10^6 B16F10 or L929 cells treated *in vitro* and from 50 mg of tumor tissue samples from each mouse group utilizing an RNA extraction kit (Favorgen Biotech Corp, South Korea), according to the manufacturer's instructions. The quantity and quality of the extracted RNA were assessed based on the absorbance ratio (A260/A280) and through agarose gel electrophoresis, respectively. The total RNA was stored at −70 °C until further assays were conducted. Subsequently, RNA was transcribed into cDNA using a cDNA synthesis kit (Parstus, Iran). The expression levels of CXCR4 and CCR5 mRNA were quantified using a SYBR Green real-time PCR assay. β-ACTIN mRNA served as an endogenous housekeeping control for all genes analyzed. All experiments were performed in triplicate, and the primers were designed using AlleleID 6.0 software (Table 3).

Statistical analysis

Data analyses were performed using R programming environment (version 4.4.1), key functions included WGCNA for co-expression networks, survminer/pROC for survival analyses, and Bioconductor (version 17). Statistical evaluations were performed with GraphPad Prism 5.0 software (GraphPad Software, Inc., La Jolla, CA, USA). Comparisons between the two groups were assessed using the Student's t-test, with p-values <0.05 considered indicative of statistically significant differences. Univariate Cox proportional hazards regression was performed for each gene to identify prognostic hub genes. Multiple testing correction was applied using the Benjamini-Hochberg method to control the FDR. Genes with adjusted p-value (FDR) < 0.05 were considered statistically significant and were used for further multivariate analysis.

Clinical characteristics of patients included in the TCGA-SKCM cohort are summarized in (Supplementary Table 1). For variables such as age, gender, race, and TNM stage, missing or unannotated values were retained in descriptive summaries but were excluded from downstream modeling where appropriate. Specifically, patients with unknown age or missing clinical annotations were excluded from any statistical model involving those variables. For instance, age was reported for most patients (mean: 59 ± 16 years), but it was not used as a covariate in Cox regression analyses. TNM staging information was incomplete for 38 patients and thus not included in stage-specific survival modeling.

Results

Data preprocessing

The Recount dataset included mRNA sequencing data from 471 melanoma samples, of which 447 contained complete clinical information. Within this dataset, 106 samples were annotated as primary tumors and 368 as metastatic tumors. Due to the significantly higher number

Table 3. Primer sequences used for RT PCR to investigate the selected genes expresion

Accession number	Gene name	Primers 5' 3'
NM_007393.5	β-ACTIN	Specific forward primer: TGTTACCAACTGGGACGACA
		Specific reverse primer: GGGGTGTTGAAGGTCTCAAA
NM_009911.5	CXCR4	Specific forward primer: CGGTAACCACCACGGCTGTAGAG
		Specific reverse primer: AGCAGGGTTCCTTGTTGGAGTCATAG
NM_013653.3	CCL5	Specific forward primer: GCTGCTTTGCCTACCTCTCC
		Specific reverse primer: TCGAGTGACAAACACGACTGC

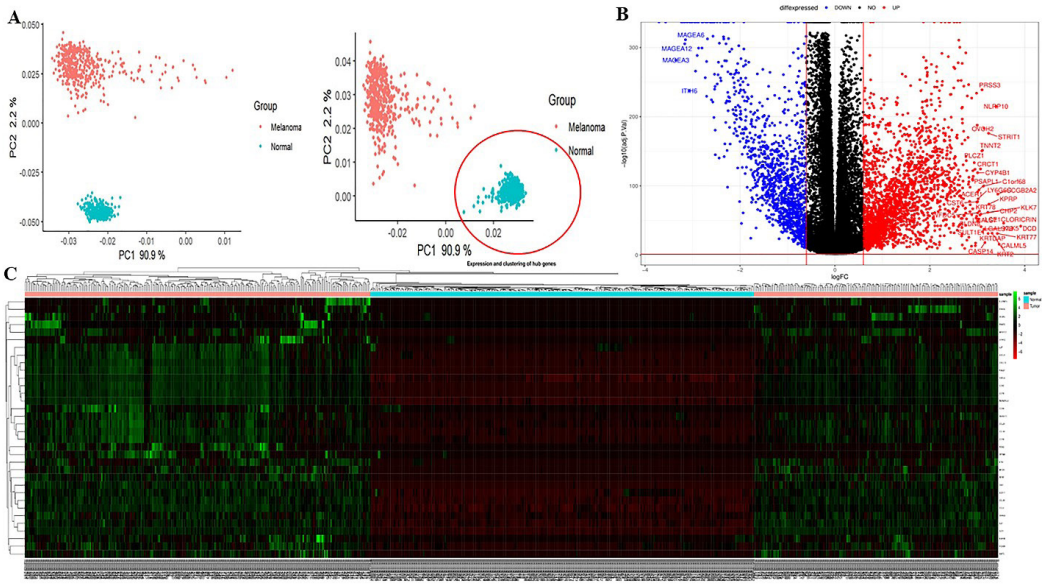

Figure 2. Data preprocessing and identification of DEGs
(A) PCA was performed on the Recount dataset using two models, and the labeled subgroup was selected for inclusion in the study. (B) Volcano plot of DEGs. (C) Hierarchical clustering heat map of expression values, with samples displayed as rows and genes as columns. The color gradient ranges from red to black to green, indicating a change in gene expression from low to high.
DEGs: Differentially expressed genes, PCA: Principal component analysis

of normal samples compared to tumor samples, PCA was performed specifically on the normal data. The dataset was divided into two subsets, from which one group was selected for analysis. Ultimately, after merging these two subsets, an expression matrix was generated that included 306 normal samples and 471 tumor samples (Figure 2A, B).

Identification of DEGs

After downloading the data from the recount, convert the gene symbols to the protein-coding of EMT. This matrix yielded a total of 996 EMT genes and 777 samples. A differential expression analysis was conducted after removing the batch effect to compare gene expression (Figure 2A, B). Limma was used to obtain DEGs, A total of 629 DEGs were identified, including 83 up-regulated genes and 546 down-regulated genes compared to the normal sample group. The DEGs were visualized in a volcano plot and a heat map (Figures 2C, D).

Relationships between co-expression modules and clinical trait

The relevant clinical trait information was obtained from TCGA datasets, and any unnecessary data was removed before conducting the analysis. At first, sample clustering was conducted to detect outliers (all samples were well clustered) (Figure 3A). The connectivity between genes in the gene network achieved a scale-free distribution when the soft threshold power beta was set to 3 (Figure 3 B, C). Then, Hierarchical cluster analysis was conducted to detect co-expression clusters with corresponding color assignments (Figure 3D). The heat map depicts the EMT-related selected genes from the Recount tumor sample WGCNA (Figure 4A). Furthermore, the eigengene

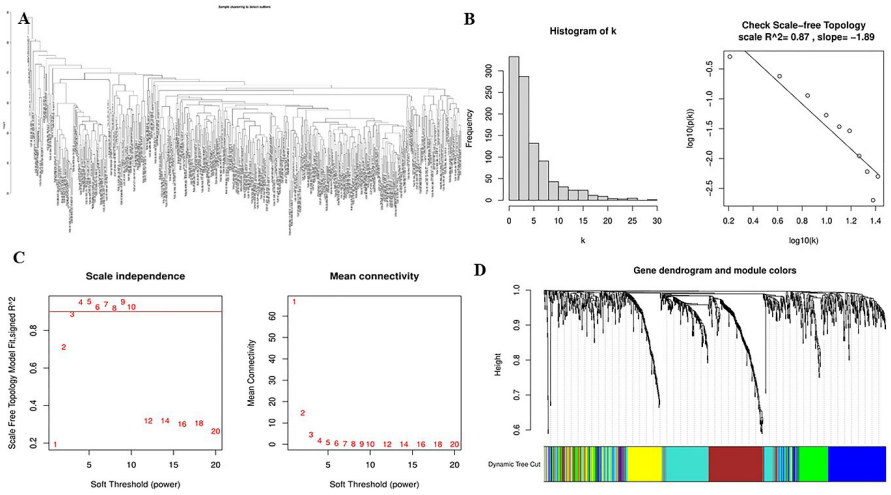

Figure 3. WGCNA analysis of EMT in TCGA tumor data
(A) Sample clustering was performed to detect outliers; all samples were well clustered. (B) The histogram of the given k and its log-log plot are presented. (C) A soft-thresholding power analysis was conducted to obtain the scale-free fit index for network topology. (D) Hierarchical cluster analysis was performed to identify co-expression clusters with corresponding color assignments. Each color represents a module in the constructed gene co-expression network created using WGCNA.
WGCNA: Weighted gene co-expression network analysis, EMT: Epithelial-mesenchymal transition, TCGA: The cancer genome atlas

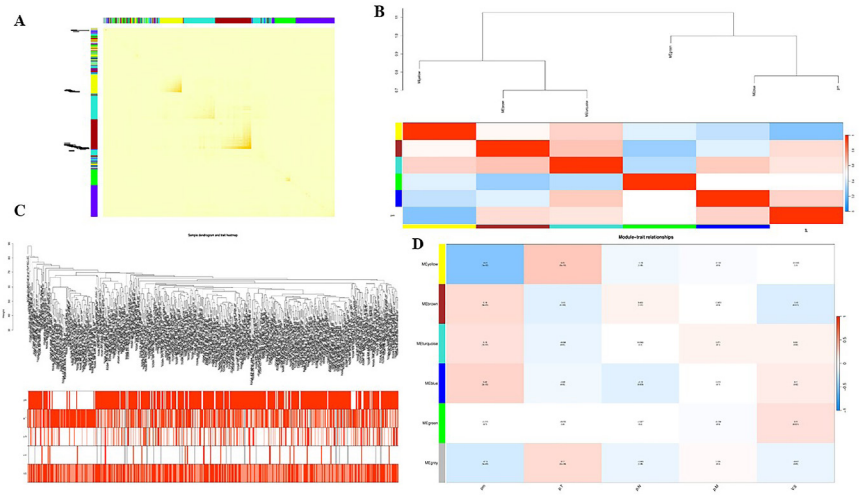

Figure 4. WGCNA analysis using TCGA clinical data
(A) The heatmap illustrates TOM among 500 randomly selected genes from the TCGA tumor sample weighted co-expression network. Lighter colors indicate lower overlap, while red indicates higher overlap. (B) This shows the clustering dendrogram of genes. The gene clustering tree (dendrogram) is generated through hierarchical clustering based on adjacency-based dissimilarity. The colored row below the dendrogram indicates module membership, as identified by the dynamic tree cut method, along with the assigned merged module colors and the original module colors. (C) This dendrogram displays the clustering of 471 SKCM samples alongside their associated clinical traits. (D) Module feature associations are shown here. Each row corresponds to a module eigengene, and each column corresponds to a clinical feature. Each cell contains the correlation in the first line and the P-value in the second line. The table is color-coded according to the correlation, as indicated by the color legend.
WGCNA: Weighted gene co-expression network analysis, TCGA: The cancer genome atlas, TOM: Topological overlap matrix, SKCM: Skin cutaneous melanoma

dendrogram and heatmap were used to demonstrate groups of correlated eigengenes (Figure 4 B, C). The relationships between the co-expression modules and the clinical traits were assessed by calculating the correlations between the module eigengenes and the clinical traits (Figure 4D). The gene list of the brown and turquoise co-expression modules was shown in (Supplementary Table 2).

Module preservation and finding the best module

Preservation analysis using WGCNA was conducted on 996 EMT genes from 306 normal samples obtained from the recount. This analysis identified five co-expressed modules, while the "grey" module was reserved for genes that were found not to be co-expressed (Figure 5A). A list of genes in each module was provided in (Supplementary Table 2). The brown and turquoise modules were determined to be non-preserved, as indicated by their Z-summary statistics being below 2. The analysis revealed these non-preserved brown and turquoise modules. As a result, these modules were selected for further investigation as modules of interest

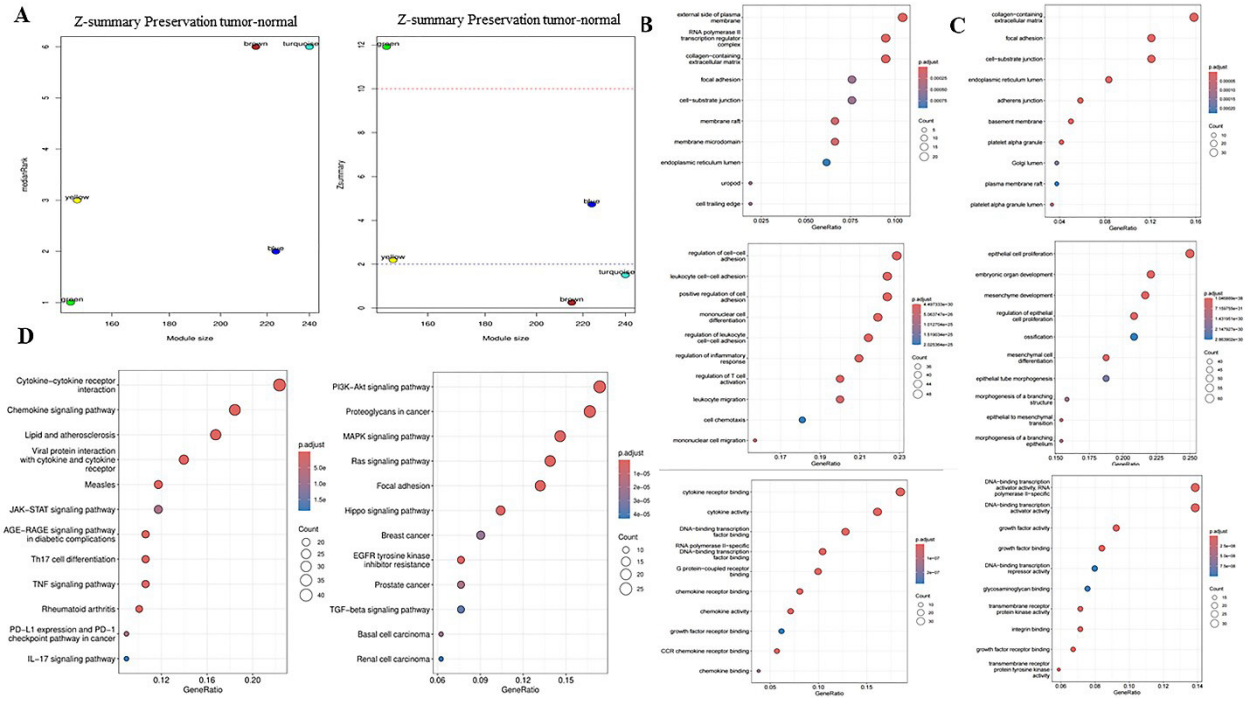

Figure 5. Module preservation and module enrichment
(A) The median rank graph on the left shows that a median rank close to zero indicates a high degree of module preservation. In the preservation Z-summary graph on the right, the dashed blue and green lines represent the thresholds at Z = 2 and Z = 10, respectively. The horizontal lines indicate the Z-summary thresholds for strong evidence of preservation (above 10) and low to moderate evidence of preservation (above 2). (B) The dot plot for the GO associated with the brown module includes BP, CC, and MF. (C) The dot plot for the GO associated with the turquoise module also includes BP, CC, and MF. (D) The top 10 enriched KEGG pathway terms for the brown module (left) and the turquoise module (right)
GO: Gene ontology, BP: Biological processes, CC: Cellular components, MF: Molecular functions, KEGG: Kyoto encyclopedia of genes and genomes

in subsequent analyses related to clinical features.

Over-representation analysis

A total of 217 genes from the brown module and 245 genes from the turquoise module were mapped using the ClusterProfiler R package and underwent GO functional and KEGG pathway enrichment analyses (41). The GO enrichment analysis for biological process (BP) terms in the brown module revealed that these genes were primarily involved in the regulation of cell-cell adhesion, leukocyte cell-cell adhesion, and the positive regulation of cell adhesion. In terms of cellular component (CC) analysis, the genes in the brown module were mainly enriched in the external side of the plasma membrane, the RNA polymerase II transcription regulator complex, and processes related to collagen-containing extracellular matrices. The GO enrichment analysis for molecular function (MF) terms indicated that the genes in the brown module were enriched in processes such as cytokine receptor binding, cytokine activity, and DNA-binding transcription factor binding (Figure 5B). The KEGG pathway enrichment analysis showed that genes in the brown module were significantly enriched in the cytokine-cytokine interaction, chemokine signaling pathway, and pathway in cancer. Among them, 27 genes in the brown module were significantly enriched in the pathway of cancer (Figure 5D).

GO enrichment analysis of biological process (BP) terms for the Turquoise module revealed that these genes were primarily enriched in the regulation of epithelial cell proliferation, embryonic organ development, and mesenchyme development. The analysis of cellular component (CC) terms indicated that the genes in the Turquoise module were mainly enriched in the collagen-containing extracellular matrix, focal adhesion, and cell-substrate junction processes. Additionally, the analysis of molecular function (MF) terms showed that the genes in the Turquoise module were enriched in DNA-binding transcription activator activity, RNA polymerase II-specific functions, and growth factor activity (Figure 5C). The KEGG pathway enrichment analysis showed that genes in the Turquoise module were significantly enriched in the Pathways in cancer, Proteoglycans in cancer, PI3K-Akt signaling pathway, Focal adhesion, and Ras signaling pathway. Among them, 24 genes of the Turquoise module were significantly enriched in the metabolic pathways (Figure 5D). DEG genes enrichment data were presented in (supplementary Figure 1).

PPI network and selected hub gene

The PPI network was constructed for the brown and turquoise modules, which included 217 and 245 genes. The top 30 genes were selected based on their degree by *CytoHubba* (Figure 6A, B). Subsequently, a Venn diagram was created using the Venny 2.1 web tool to compare the selected genes from the brown and turquoise modules with the DEG identified between normal and tumor data. Out of the 30 important genes from each module, 24 were found to overlap with the DEG. A total of 48 unique genes were obtained from this analysis (Figure 6C).

Validation of hub genes by expression level in GEO

The mRNA expression levels of the 48 hub genes were

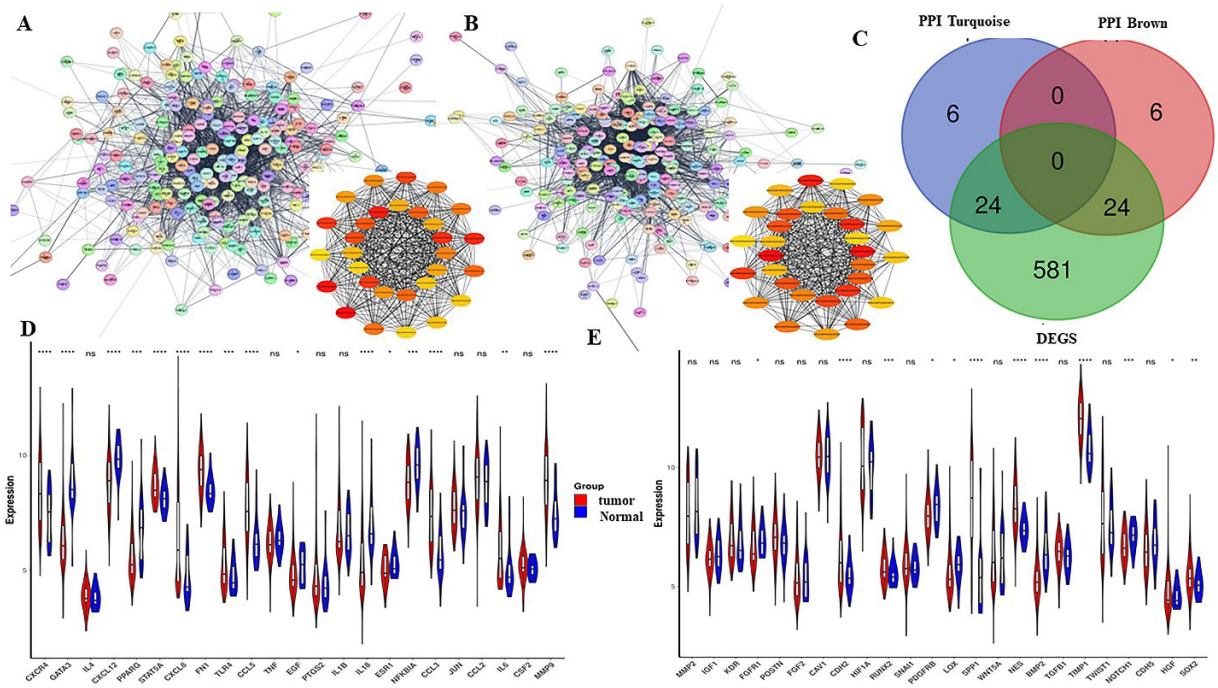

Figure 6. Hub gene selection was performed as follows:
(A) A PPI network was constructed for the genes in the turquoise module. We selected 30 genes based on their degree within this network. (B) Similarly, a PPI network was created for the genes in the brown module, and again, 30 genes were selected according to their degree. (C) A Venn diagram illustrated that the 30 selected genes from the turquoise and brown modules had 24 overlapping genes that were differentially expressed between normal samples from the GTEx database and melanoma samples from TCGA. (D) A box plot displayed the gene expression levels of the 24 selected genes from the brown module using GEO data. (E) Another box plot represented the gene expression levels of the same 24 selected genes from the brown module, with red indicating the tumor group and blue indicating the normal group
The X-axis represented the related genes from 24 EMT, while the Y-axis showed the expression levels of those genes. The Wilcoxon test was utilized to assess the differences in gene expression between the tumor and normal groups, with $P<0.05$ indicating statistical significance; *$P<0.05$, **$P<0.01$, and ***$P<0.001$. The data came from the TCGA and GTEx Project.
PPI: Protein-protein interaction, GTEx: Genotype-tissue expression, TCGA: The cancer genome atlas, GEO: Gene expression omnibus, EMT: Epithelial-mesenchymal transition

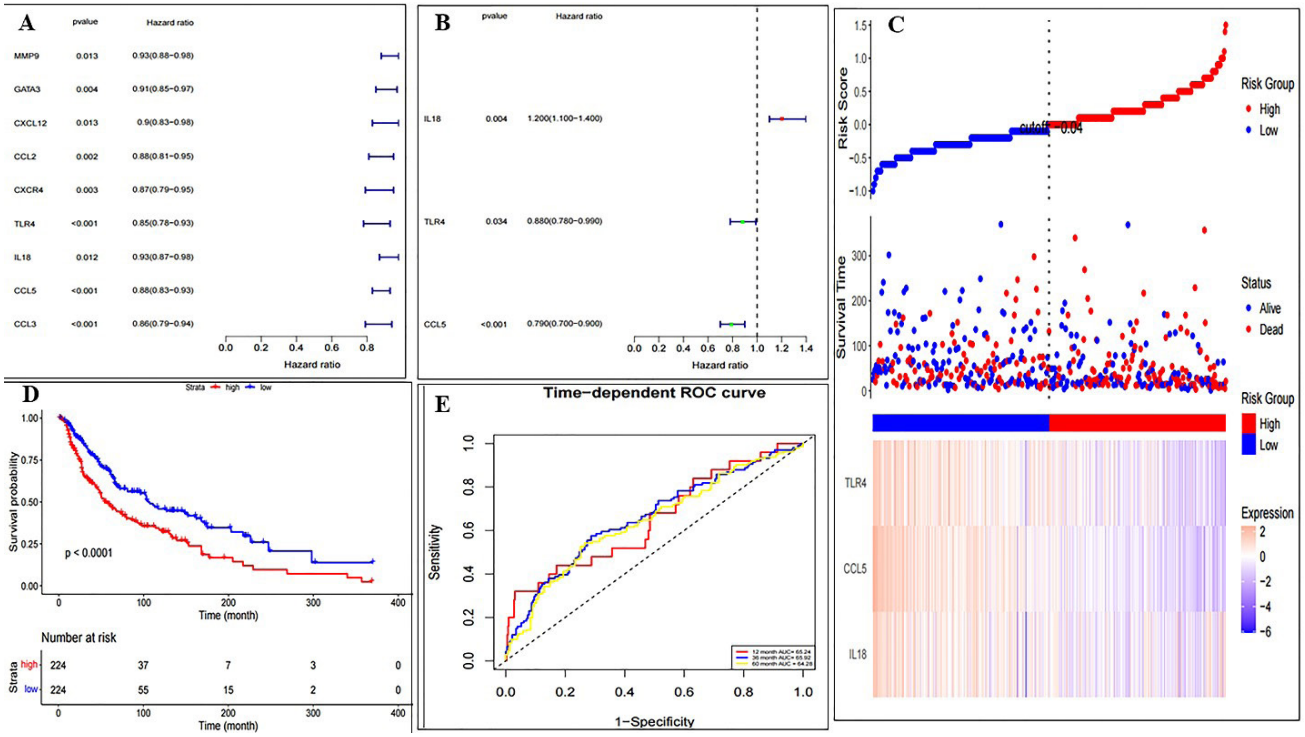

Figure 7. Survival analysis by Cox risk score analysis, Kaplan–Meier analysis, and time-dependent ROC analysis for the validation of the prognostic model (A) Forest plot for the results of univariate Cox regression analysis in 13 significant genes. (B) Forest plot for the result of multivariate Cox regression analysis. (C) The rank of risk score and distribution of groups. Melanoma patients were divided into low- and high-risk subgroups based on the median value of the risk score calculated. (D) Kaplan–Meier curve of melanoma patients by risk score, and (E) time-dependent ROC analysis.
ROC analysis: Receiver operating characteristic analysis

analyzed using the GEO validation dataset. Ultimately, 13 hub genes were selected that showed a significant increase in expression in tumor samples compared to normal samples (Figure 6D, E).

Survival analysis

Development of a prognostic classifier by performing univariabel Cox regression analysis (adjusted q-values <0.05) in the 13 genes, found that 9 genes were survival-associated (Figure 7A). Multivariabel cox regression analysis was employed to identify a total of 3 prognostic hub genes including CCL5, IL18, TLR4 (Figure 7B). Subsequently, the coefficient was extracted from the results of multivariabel Cox regression and calculated individualized risk scores with coefficient-weighted expression levels of 3 prognostic genes. Based on the median risk score, melanoma samples were divided into low-risk (n = 224) and high-risk groups (n = 224). The distribution of risk score, survival status, and expression of the three hub genes was exhibited in (Figure 7C). Besides, the survival analysis showed that the survival rate in the low-risk group was remarkably prolonged than those in the high-risk group (Figure 7D). ROC curve analyses showed that these genes exhibited diagnostic efficiency for melanoma patients (Figure 7E). ROC curve analysis showed that the risk score had a moderate discriminative ability, with an AUC of 0.65 at 1 year, 0.65 at 3 years, and 0.64 at 5 years. Based on the literature review and bioinformatics findings, CCL5 and CXCR4 were selected for experimental validation in melanoma cell treatments in this study.

Correlation between the expression hub genes and pathological stages and primary/metastatic stat in melanoma

Using the GEPIA 2.0 web server, the correlation between the expression of the two selected hub genes and different pathological stages of melanoma was analyzed. CXCR4 and CCL5 were found to be significantly up-regulated in melanoma samples compared to normal controls, and significant differences in their expression were also observed across different tumor stages (Figure 8A). Four stages were represented in this plot: stage 1, stage 2, stage 3, and stage 4. The UALCAN web server was utilized to analyze the correlation between gene expression and both primary and metastatic states of melanoma, using TCGA data (Figure 8B). Then, the correlation of CCL5 and CXCR4 expression was evaluated between melanoma metastatic and primary samples in the Recount expression matrix in this study. These boxplots show the relationship between the expression level of CCL5, CXCR4, and metastatic melanoma (Figure 8C). Consequently, these two genes were nominated for further investigation in the laboratory phase.

Combination treatment selectively induced cellular damage in B16F10 cells

Metabolic activity was assessed using the MTT assay after cell treatment with CAP (40 sec) and Anti-PD-1 (100 µg/ml). **T**hese treatment conditions were selected based on preliminary dose- and time-response experiments (CAP: 30–120 s; Anti-PD-1: 10–250 µg/mL), which were conducted to identify biologically effective conditions and are presented in the (Supplementary Figure 2-4**).**

The treatments with CAP and the combination therapy resulted in a significant reduction in metabolically active B16F10 cells when compared to the untreated group. In contrast, treatment with Anti-PD-1 showed a lesser reduction in metabolically active B16F10 cells compared to the untreated controls. Notably, all treatment groups suggested no significant effect on the L929 cells (Figure 9A).

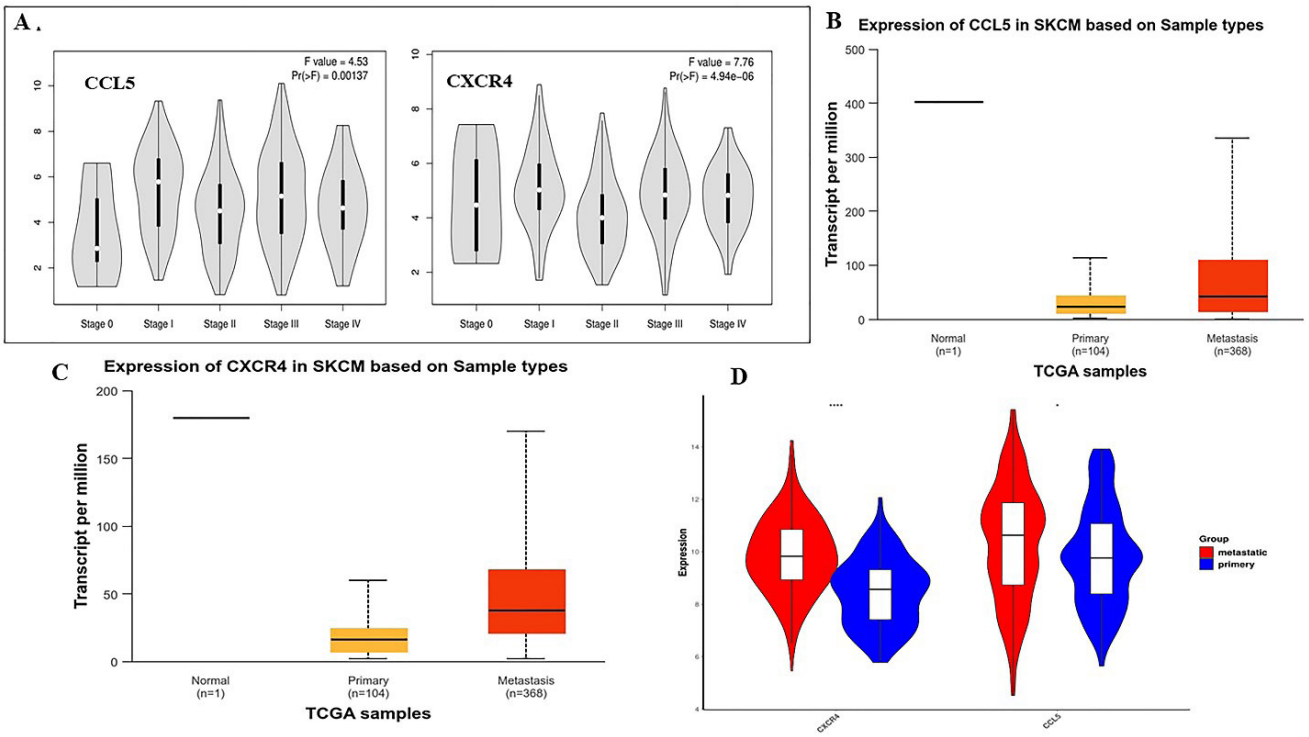

Figure 8. There is a significant correlation between the expression of hub genes and both the pathological stage and primary metastatic state of melanoma
(A) The expression levels of CCL5 and CXCR4 show a significant correlation with the pathological stage of melanoma, as analyzed using GEPIA2. (B, C) There is also a significant correlation in the expression of CCL5 and CXCR4 between metastatic and primary melanoma samples. The boxplots illustrate the relationship between the expression levels of CCL5 and CXCR4 in metastatic melanoma from human tumors, utilizing data obtained from ULCAN. (D) Furthermore, the boxplots demonstrate a significant correlation in the expression of CCL5 and CXCR4 between metastatic and primary melanoma samples based on our expression matrix from this study.
GEPIA2: Gene expression profiling interactive analysis 2; ULCAN: University of lisbon cancer network

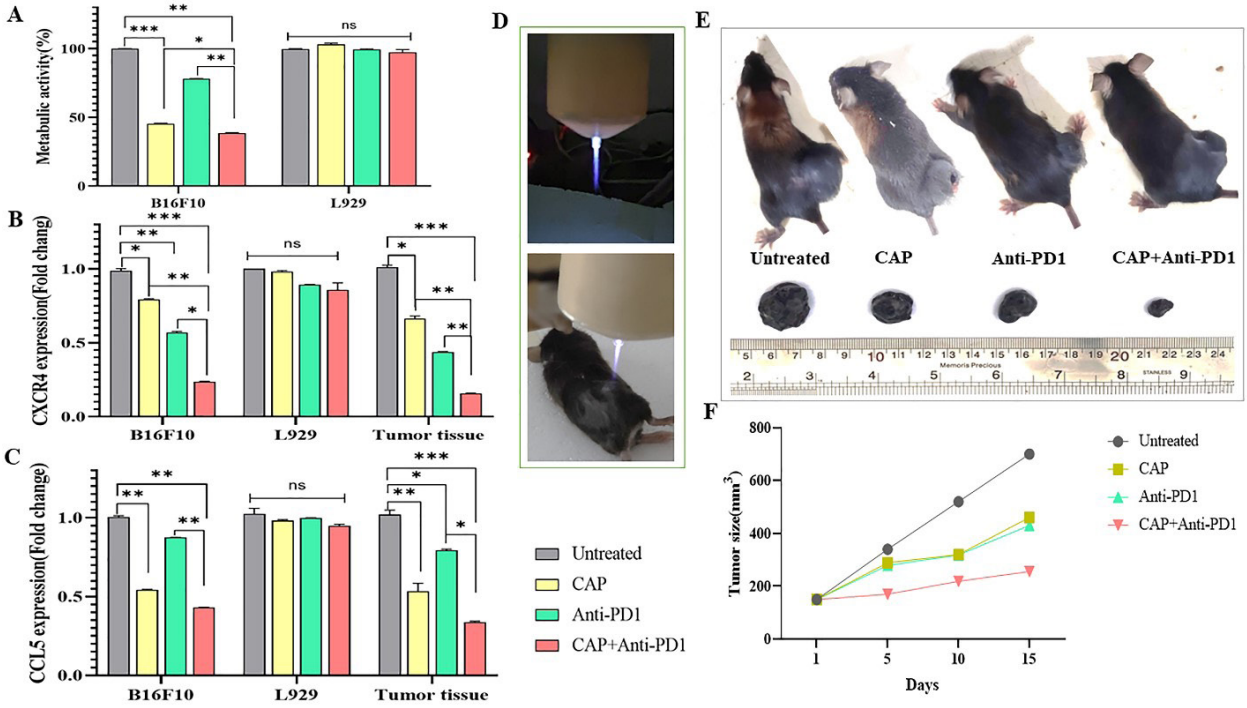

Figure 9. Effect of CAP and Anti-PD-1 monotherapy and combination therapy on melanoma *in vitro* and *in vivo*
B16F10 melanoma cells and L929 fibroblasts were left untreated or treated with CAP, Anti-PD-1, or the CAP + Anti-PD-1 combination. (A) Metabolic activity of B16F10 and L929 cells assessed by MTT assay following CAP exposure (45 s) and/or Anti-PD-1 treatment (100 µg/ml). (B, C) Relative mRNA expression levels of CXCR4 and CCL5 measured by real-time PCR in B16F10 cells, L929 fibroblasts, and excised tumor tissues. (D) Representative images showing CAP application to melanoma-bearing mice. (E) Photographs of tumor-bearing mice and excised tumors from each treatment group (Untreated, CAP, Anti-PD-1, CAP + anti-PD-1). (F) Tumor growth curves illustrating tumor volume changes on days 1, 5, 10, and 15 post-treatment, showing the most pronounced tumor regression in the combination-therapy group.
Data represent mean ± SD (n = 3 independent experiments for *in vitro* assays; n = 3 mice per group for *in vivo* assays). Statistical significance was defined as $P<0.05$; * $P<0.05$, ** $P<0.01$, *** $P<0.001$; ns, not significant.
CAP: Cold atmospheric plasma

Combination treatment reduces the CXCR4 and CCL5 as an EMT marker in B16F10 and melanoma tumor tissue

Real-time PCR assay was performed to assess gene expression levels across different treatment conditions, including CAP, Anti-PD-1, and their combination (CAP+Anti-PD-1). CAP treatment significantly reduced CCL5 expression levels of B16F10 and melanoma tumor tissue. Anti-PD-1 treatment caused a smaller reduction, while the combination therapy (CAP+Anti-PD-1) exhibited the strongest effect. In L929 cells, gene expression remained largely unaffected across treatments (Figure 9B). In untreated B16F10 cells and in the untreated group of the mouse model, baseline CXCR4 expression was high. CAP treatment reduced CXCR4 expression, Anti-PD-1 treatment led to a further reduction, and the combination resulted in the strongest down-regulation in both B16F10 melanoma cells and melanoma tumor tissues. In contrast, L929 normal fibroblasts exhibited only minimal changes in CXCR4 expression across treatment conditions (Figure 9C).

Combination treatment induced tumor regression in B16F10 melanoma-bearing mice

To evaluate the *in vivo* efficacy of the combination therapy on tumor regression, tumor progression was monitored by measuring tumor size and performing gene expression analysis. No significant differences in tumor size were observed among the groups at the start of the intervention. However, following the initiation of CAP, Anti-PD-1, or combination therapy on days 5, 10, and 15, tumor sizes were significantly reduced compared with the untreated group from day 5 onward. Among the treatment modalities, the combination therapy suggested the most pronounced effect on suppressing tumor progression (Figure 9D-F).

Discussion

The global incidence of melanoma has steadily increased over the past three decades. Melanoma is a highly aggressive and treatment-resistant form of skin cancer, underscoring the critical importance of early diagnosis and timely intervention to improve prognosis and survival rates (2, 3). Among the therapeutic approaches for melanoma, Anti-PD-1 therapy is commonly employed, as it binds to PD-1 receptors on both cancer and immune cells, thereby inhibiting tumor growth while simultaneously enhancing immune cell activity (11, 12). As a complementary treatment with fewer side effects, CAP devices have shown considerable promise in cancer therapy. CAP can generate ROS and RNS that have been shown to selectively affect cancer cells (16). The application of CAP has been reported to induce cancer cell death and could augment immune response to cancer cells (13, 14). This immune response can be further enhanced through the use of Anti-PD-1 therapy. Moreover, findings from previous research suggest that the application of CAP and Anti-PD-1 alone can reduce EMT in cancer cells (22, 23). EMT is widely recognized as a critical mechanism contributing to tumor invasion, and metastasis, and contributing to drug resistance (24).

In this research, a novel EMT-related gene signature associated with melanoma prognosis was identified through an integrative bioinformatics approach. Transcriptomic data from Recount, and GEO were analyzed to identify differentially expressed EMT-related genes, followed by WGCNA to determine the most relevant gene modules. Further survival analysis and validation steps led to the identification of key prognostic genes, which were experimentally assessed. These genes were evaluated as significant prognostic markers in melanoma before and after treatment with CAP and Anti-PD-1, highlighting their potential role in predicting therapeutic outcomes in melanoma.

Bioinformatics analysis suggested that CCL5 was significantly up-regulated in melanoma samples when compared to normal tissues, showing a strong correlation with metastatic progression. Both univariable and multivariable Cox regression models further validated their prognostic significance, emphasizing their potential role in patient stratification. Supporting this finding, a 2018 study reported that elevated CCL5 expression was associated with promotion of the EMT process in cancer cells, thereby contributing to metastasis and resistance to therapy (52).

Experimental results from this study suggested that CAP treatment significantly reduced CCL5 expression in B16F10 melanoma cells, and this effect was further enhanced when combined with Anti-PD-1 therapy. A similar pattern was observed in melanoma tumor tissues, where the combination therapy resulted in the most pronounced down-regulation of CCL5 compared with either treatment alone. In contrast, normal fibroblasts showed only minimal changes in CCL5 expression across treatment conditions, suggesting that CAP and Anti-PD-1 specifically targeted tumor cells while sparing normal tissues. This finding aligns with a previous study by Saadati and her colleagues, which indicated that CAP treatment might exert immunomodulatory effects by decreasing CCL5 expression, a marker linked to poor prognosis in cancers (53). Additionally, research conducted by Exposito *et al.* demonstrated that combining CCR5 antagonists, such as maraviroc, with immune checkpoint inhibitors like Anti-PD-1 has the potential to enhance the efficacy of immunotherapy by disrupting tumor-promoting pathways (54).

In this study, bioinformatic analysis indicated that, similar to CCL5, CXCR4 was significantly up-regulated in melanoma samples, particularly in metastatic cases. Survival analyses showed that CXCR4 expression was correlated with OS in melanoma patients, underscoring its potential as a prognostic marker. These findings were consistent with previous studies demonstrating the critical role of CXCR4 in cancer, where its binding to CXCL12 activated downstream signaling pathways that promoted cancer cell proliferation and metastasis (55, 56). Additionally, research conducted by Longo-Imedio *et al.* has shown that CXCR4 expression in malignant melanoma predicts poor survival rates and higher metastatic potential (57). Given the vital role of the CXCR4/CXCL12 axis in various cancers, including melanoma (58), there has been considerable interest in discovering and developing therapies that target and inhibit this axis (59).

Experimental results from this study indicated that CAP treatment led to a significant reduction in CXCR4 expression in B16F10 melanoma cells, an effect that was further enhanced when combined with Anti-PD-1 therapy. A similar trend was observed in tumor tissues, where the combination therapy resulted in the most pronounced suppression of CXCR4. Notably, in L929 cells, the treatment had minimal impact on CXCR4 expression, further supporting the tumor-specific effects of CAP and Anti-PD-1 therapy. These findings were consistent with previous studies; for instance, a 2015 investigation on CXCR4 reported that RNA interference–mediated knockdown of

the CXCR4 gene significantly reduced tumor growth and metastasis both *in vitro* and *in vivo* (60). CAP, recognized as a promising therapeutic approach, has suggested its potential to induce apoptosis, inhibit cell proliferation, and alter gene expression profiles critical for metastasis and EMT in cancer cells, underscoring its value in targeting EMT-associated genes (21).

Moreover, research indicates that Anti-PD-1 therapy may also indirectly affect CXCR4 expression on tumor cells by modifying the tumor microenvironment. Enhanced T-cell activity resulting from Anti-PD-1 therapy can lead to increased production of cytokines like interferon-gamma (IFN-γ) (61). Katayama and colleagues noted that IFN-γ can, in turn, modulate the expression of various genes, potentially including those related to CXCR4 (62). Furthermore, a 2019 study by D'Alterio *et al.* suggested that PD-1 blockade might reduce CXCR4 expression, which could, in turn, diminish tumor cell migration and metastasis (61).

The MTT assay results supported these observations by demonstrating a marked reduction in the viability of B16F10 melanoma cells following CAP exposure, with an even greater decrease observed under combined CAP and Anti-PD-1 treatment. Importantly, viability changes in L929 fibroblasts were minimal, reinforcing the tumor-selective nature of CAP-based therapy. CAP is thought to exert its cytotoxic effects primarily through the generation of RONS, which induce oxidative stress, DNA damage, mitochondrial dysfunction, and caspase-dependent apoptosis in cancer cells while sparing normal cells with stronger antioxidant defenses (16, 63). In addition to its well-established role in immune evasion, recent evidence indicates that melanoma cells themselves can express PD-1, where its engagement activates pro-survival and pro-metastatic signaling pathways such as PI3K/AKT and MAPK. The possibility that PD-1 expressed directly on melanoma cells contributes to tumor growth and metastasis has been reported in prior studies (11). Thus, the synergy observed in our MTT assays may reflect the combined actions of CAP-induced oxidative damage and the direct inhibition of tumor-intrinsic PD-1 signaling, providing complementary mechanisms through which Anti-PD-1 therapy augments CAP's anti-tumor effects. suggesting complementary mechanisms at play. To further evaluate this synergistic effect *in vivo* in the presence of an intact immune system, we assessed the expression of the selected candidate genes in tumor tissues from the mouse model, which confirmed our *in vitro* findings.

A strong concordance was observed between our *in vitro* and *in vivo* findings regarding CCL5 and CXCR4 expression. In B16F10 melanoma cells, CAP treatment led to a significant down-regulation of both CCL5 and CXCR4, an effect that was further enhanced when combined with Anti-PD-1 therapy. Similarly, in the mouse melanoma model, tumor tissues treated with the combination therapy exhibited the most pronounced suppression of these genes compared with either monotherapy, confirming the synergistic effect under physiological conditions. Notably, although the magnitude of down-regulation was slightly greater *in vitro* likely due to the absence of stromal interactions and immune components the overall pattern of combined CAP and Anti-PD-1 producing the strongest inhibitory effect was consistent across experimental contexts. This alignment between cellular and animal data strengthens the evidence that targeting EMT-associated genes such as CCL5 and CXCR4 through CAP and PD-1 blockade may effectively limit melanoma progression and metastasis in a tumor-selective manner.

In general, the results of this study indicated that bioinformatics analyses provided valuable insights into the molecular mechanisms underlying the observed effects. WGCNA identified CCL5 and CXCR4 as key genes within distinct co-expression modules that were enriched in EMT-related pathways, including cytokine signaling and focal adhesion networks. GO and KEGG pathway analyses further emphasized their roles in tumor-promoting processes. Experimental validation confirmed that these genes were not only differentially expressed in melanoma but also responded to a combination of CAP and Anti-PD-1 therapy in both *in vitro* and *in vivo* models. The selective down-regulation of CCL5 and CXCR4 in tumor cells and tissues, while sparing normal fibroblasts, underscored the potential of combination therapy as a targeted approach for melanoma treatment.

Conclusion

This study demonstrated that combining CAP with Anti-PD-1 therapy was more effective against melanoma than either treatment alone. The combination reduced the viability of B16F10 melanoma cells *in vitro* and suppressed tumor growth in melanoma-bearing mice *in vivo*, while sparing normal fibroblasts, indicating a tumor-selective action. It also markedly down-regulated the EMT-associated biomarkers CCL5 and CXCR4, which are closely linked to metastatic potential and poor prognosis, suggesting that modulation of these genes may represent one mechanism underlying the observed therapeutic effect. Together, these findings support the potential of CAP to enhance the effectiveness of ICB and highlight the relevance of CCL5 and CXCR4 pathways as promising targets for melanoma therapy.

Acknowledgment

The authors gratefully acknowledge the student research committee of Mazandaran University of Medical Science, Sari, Iran, for financially supporting this research.

Limitations and Future Directions

Despite the promising results, this study has some limitations. Future studies should explore the upstream regulatory networks governing these gene expressions and assess potential combinatorial strategies with other immune checkpoint inhibitors. The *in vivo* experiments were conducted as a pilot study with three mice per group without formal power analysis or randomization. Although sufficient for exploratory purposes, these sample sizes limit the statistical power and generalizability of the findings.

Data Availability Statement

All datasets, software, plugins, versions, and methodology are described in detail in the manuscript; additional detailed analysis spreadsheets and information are included in the supplementary material. A specific clarification or analysis file will be made available upon request.

The datasets analyzed during the current study are publicly available at: Recount: https://jhubiostatistics.shinyapps.io/recount/, GEO: GSE15605, GSE46517, GSE7553

Ethics Approval

Ethics approval of this study is (IR.MAZUMS.4.REC.1402.18172).

Funding

This study was financially supported by a grant (grant number: 18172) from the Research and Technology Council of Mazandaran University of Medical Sciences, Iran.

Authors' Contributions

Z R and A R designed the study. Z R, F B, M E, and M M performed experiments and collected data. Z R and F A carried out formal analysis, methodology, and software. Z R prepared the draft manuscript and visualization. F B, M E, F A, Z Y, and G R reviewed and edited the manuscript. A R supervised and critically revised the article. Z R, F A, F B, M E, M M, Z Y, G R, and A R approved the final version of the manuscript.

Conflicts of Interest

The authors declare that they have no known competing financial interests or personal relationships that could have appeared to influence the work reported in this paper. The authors declare that they have no conflict of interest.

Declaration

We have not used any AI tools or technologies to prepare this manuscript.

References

1. Sánchez-Sancho P, Alonso-Martínez C, Renedo-Miró B. Tratamiento con nivolumab en una paciente oncológica trasplantada. El Farmacéutico Hospitales 2022.
2. Sung H, Ferlay J, Siegel RL, Laversanne M, Soerjomataram I, Jemal A, *et al.* Global cancer statistics 2020: GLOBOCAN estimates of incidence and mortality worldwide for 36 cancers in 185 countries. CA Cancer J Clin 2021; 71:209-249.
3. Eddy K, Shah R, Chen S. Decoding melanoma development and progression: Identification of therapeutic vulnerabilities. Front Oncol 2021; 10:626129.
4. Lee L, Ramos-Alvarez I, Jensen RT. Predictive factors for resistant disease with Medical/Radiologic/Liver-directed anti-tumor treatments in patients with advanced pancreatic neuroendocrine neoplasms: Recent advances and controversies. Cancers 2022; 14:1250.
5. Sone K, Kukita A, Masui Y, Yamada D, Shinozaki-Ushiku A, Kawata A, *et al.* Recurrent malignant melanoma of the uterine cervix treated with anti-PD-1 antibodies and anti-CTLA-4 antibodies: a case report. Mol Clin Oncol 2022; 16:63.
6. McArthur GA, Chapman PB, Robert C, Larkin J, Haanen JB, Dummer R, *et al.* Safety and efficacy of vemurafenib in BRAFV600E and BRAFV600K mutation-positive melanoma (BRIM-3): Extended follow-up of a phase 3, randomised, open-label study. Lancet Oncol 2014; 15:323-332.
7. Sagwal SK, Pasqual-Melo G, Bodnar Y, Gandhirajan RK, Bekeschus S. Combination of chemotherapy and physical plasma elicits melanoma cell death via upregulation of SLC22A16. Cell Death Dis 2018; 9:1179.
8. Hachey SJ, Boiko AD. Therapeutic implications of melanoma heterogeneity. Exp Dermatol 2016; 25:497-500.
9. Ribas A, Wolchok JD. Cancer immunotherapy using checkpoint blockade. Science 2018; 359:1350-1355.
10. Zou W, Wolchok JD, Chen L. PD-L1 (B7-H1) and PD-1 pathway blockade for cancer therapy: Mechanisms, response biomarkers, and combinations. Sci Transl Med 2016; 8:328rv4
11. Kleffel S, Posch C, Barthel SR, Mueller H, Schlapbach C, Guenova E, *et al.* Melanoma cell-intrinsic PD-1 receptor functions promote tumor growth. Cell 2015; 162:1242-1256.
12. Tone M, Iwahori K. PD-1 expression on tumor cells: A new target for cancer therapy. Transl Lung Cancer Res 2024; 13:186-189.
13. Mateu-Sanz M, Ginebra M-P, Tornín J, Canal C. Cold atmospheric plasma enhances doxorubicin selectivity in metastasic bone cancer. Free Radic Biol Med 2022; 189:32-41.
14. Mali SB. Role of Cold atmospheric plasma in cancer management. Oral Oncology Reports 2024; 9:100133.
15. Khalaf AT, Abdalla AN, Ren K, Liu X. Cold atmospheric plasma (CAP): A revolutionary approach in dermatology and skincare. Eur J Med Res 2024; 29:487.
16. Babajani A, Eftekharinasab A, Bekeschus S, Mehdian H, Vakhshiteh F, Madjd Z. Reactive oxygen species from non-thermal gas plasma (CAP): implication for targeting cancer stem cells. Cancer Cell International 2024; 24:344.
17. Khalaf AT, Abdalla AN, Ren K, Liu X. Cold atmospheric plasma (CAP): A revolutionary approach in dermatology and skincare. Eur J Med Res 2024; 29:487.
18. Philippou Y, Sjoberg HT, Murphy E, Alyacoubi S, Jones KI, Gordon-Weeks AN, *et al.* Impacts of combining anti-PD-L1 immunotherapy and radiotherapy on the tumour immune microenvironment in a murine prostate cancer model. Br J Cancer 2020; 123:1089-1100.
19. Cao Y, Ye Q, Ma M, She QB. Enhanced bypass of PD-L1 translation reduces the therapeutic response to mTOR kinase inhibitors. Cell Rep 2023; 42:112764.
20. Chen G, Chen Z, Wen D, Wang Z, Li H, Zeng Y, *et al.* Transdermal cold atmospheric plasma-mediated immune checkpoint blockade therapy. Proceedings of the National Academy of Sciences 2020; 117:3687-3692.
21. Zhuang J, Yuan Q, Chen C, Liu G, Zhong Z, Zhu K, *et al.* Nanosecond pulsed cold atmospheric plasma jet suppresses proliferation and migration of human glioblastoma cells via apoptosis promotion and EMT inhibition. Arch Biochem Biophys 2023; 747:109757.
22. Messeha SS, Zarmouh NO, Soliman KF. Polyphenols modulating effects of PD-L1/PD-1 checkpoint and EMT-mediated PD-L1 overexpression in breast cancer. Nutrients 2021; 13:1718.
23. Wang L, Saci A, Szabo PM, Chasalow SD, Castillo-Martin M, Domingo-Domenech J, *et al.* EMT-and stroma-related gene expression and resistance to PD-1 blockade in urothelial cancer. Nat Commun 2018; 9:3503.
24. Nieto MA. The ins and outs of the epithelial to mesenchymal transition in health and disease. Annu Rev Cell Dev Biol 2011; 27:347-376.
25. Ye X, Weinberg RA. Epithelial–mesenchymal plasticity: A central regulator of cancer progression. Trends Cell Biol 2015; 25:675-686.
26. Coricovac D, Dehelean C, Moaca E-A, Pinzaru I, Bratu T, Navolan D, *et al.* Cutaneous melanoma—a long road from experimental models to clinical outcome: A review. Int J Mol Sci 2018; 19:1566.
27. Chen X, Guo W, Xu X-j, Su F, Wang Y, Zhang Y, *et al.* Melanoma long non-coding RNA signature predicts prognostic survival and directs clinical risk-specific treatments. J Dermatol Sci 2017; 85:226-234.
28. Liu Y, Chen Y, Hu X, Meng J, Li X. Development and validation of the B cell-associated fc receptor-like molecule-based prognostic signature in skin cutaneous melanoma. Biomed Res Int 2020; 2020:8509805.
29. Consortium G, Ardlie KG, Deluca DS, Segrè AV, Sullivan TJ, Young TR, *et al.* The genotype-tissue expression (GTEx) pilot analysis: Multitissue gene regulation in humans. Science 2015; 348:648-660.
30. Gentles AJ, Newman AM, Liu CL, Bratman SV, Feng W, Kim D, *et al.* The prognostic landscape of genes and infiltrating immune cells across human cancers. Nat Med 2015; 21:938-945.
31. Collado-Torres L, Nellore A, Kammers K, Ellis SE, Taub MA,

Hansen KD, *et al.* Reproducible RNA-seq analysis using recount2. Nat Biotechnol 2017; 35:319-321.
32. Liu J, Li R, Liao X, Hu B, Yu J. Comprehensive investigation of the clinical significance and molecular mechanisms of plasmacytoma variant translocation 1 in sarcoma using genome-wide RNA sequencing data. J Cancer 2019; 10:4961-4977.
33. Huang R, Mao M, Lu Y, Yu Q, Liao L. A novel immune-related genes prognosis biomarker for melanoma: Associated with tumor microenvironment. Aging (Albany NY) 2020; 12:6966-6980.
34. Zhang X, Ping S, Zhang R, Li C, Gao C, Ma H, *et al.* Development and validation of an immune-related gene pairs signature in lower-grade II/III glioma. Int J Gen Med. 2021 Nov 23;14:8611–8620
35. Xiao Y, Zhu Z, Li J, Yao J, Jiang H, Ran R, *et al.* Expression and prognostic value of long non-coding RNA H19 in glioma via integrated bioinformatics analyses. Aging (Albany NY) 2020; 12:3407.
36. Ho DW-H, Kai AK-L, Ng IO-L. TCGA whole-transcriptome sequencing data reveals significantly dysregulated genes and signaling pathways in hepatocellular carcinoma. Front Med 2015; 9:322-330.
37. Robinson MD, McCarthy DJ, Smyth GK. edgeR: A bioconductor package for differential expression analysis of digital gene expression data. Bioinformatics 2010; 26:139-140.
38. Langfelder P, Horvath S. WGCNA: An R package for weighted correlation network analysis. BMC bioinformatics 2008; 9:1-13.
39. Consortium GO. The gene ontology (GO) project in 2006. Nucleic Acids Res 2006; 34:D322-D326.
40. Kanehisa M, Goto S. KEGG: Kyoto encyclopedia of genes and genomes. Nucleic Acids Res 2000; 28:27-30.
41. Szklarczyk D, Franceschini A, Wyder S, Forslund K, Heller D, Huerta-Cepas J, *et al.* STRING v10: protein–protein interaction networks, integrated over the tree of life. Nucleic Acids Res 2015; 43:D447-D452.
42. Tang Z, Li C, Kang B, Gao G, Li C, Zhang Z. GEPIA: A web server for cancer and normal gene expression profiling and interactive analyses. Nucleic Acids Res 2017; 45:W98-W102.
43. Mondal P, Singh P, Mahanti K, Bhattacharyya S. Identification of cancer stem cell (CSC) associated genes, prognostic value and candidate drugs as modulator of CSC associated signaling in carcinomas through a multiomics data analysis approach. Informatics 2024; 11:95.
44. Appay V, Rowland-Jones SL. RANTES: A versatile and controversial chemokine. Trends Immunol 2001; 22:83-87.
45. Rafiei A, Sohbatzadeh F, Hadavi S, Bekeschus S, Alimohammadi M, Valadan R. Inhibition of murine melanoma tumor growth *in vitro* and *in vivo* using an argon-based plasma jet. Clin Plasma Med 2020; 19:100102.
46. Alimohammadi M, Golpour M, Sohbatzadeh F, Hadavi S, Bekeschus S, Niaki HA, *et al.* Cold atmospheric plasma is a potent tool to improve chemotherapy in melanoma *in vitro* and *in vivo*. Biomolecules 2020; 10:1011.
47. Yazdani Z, Mehrabanjoubani P, Rafiei A, Biparva P, Kardan M. Combined effect of cold atmospheric plasma and curcumin in melanoma cancer. Biomed Res Int 2021; 2021:1969863.
48. Capasso A, Lang J, Pitts TM, Jordan KR, Lieu CH, Davis SL, *et al.* Characterization of immune responses to anti-PD-1 mono and combination immunotherapy in hematopoietic humanized mice implanted with tumor xenografts. J Immunother Cancer 2019; 7:37.
49. Stuckey JE, Makhija SD, Reimer DC, Eswaraka JR. Effects of different grades of carbon dioxide on euthanasia of mice (Mus musculus). J Am Assoc Lab Anim Sci 2023; 62:430-437.
50. Festing MF, Altman DG. Guidelines for the design and statistical analysis of experiments using laboratory animals. ILAR J 2002; 43:244-258.
51. Dakup PP, Porter KI, Little AA, Zhang H, Gaddameedhi S. Sex differences in the association between tumor growth and T cell response in a melanoma mouse model. Cancer Immunol Immunother 2020; 69:2157-2162.
52. Song X, Zhou X, Qin Y, Yang J, Wang Y, Sun Z, *et al.* Emodin inhibits epithelial-mesenchymal transition and metastasis of triple negative breast cancer via antagonism of CC-chemokine ligand 5 secreted from adipocytes. Int J Mol Med 2018; 42:579-588.
53. Saadati F, Moritz J, Berner J, Freund E, Miebach L, Helfrich I, *et al.* Patient-derived human basal and cutaneous squamous cell carcinoma tissues display apoptosis and immunomodulation following gas plasma exposure with a certified argon jet. Int J Mol Sci 2021; 22:11446.
54. Exposito F, Redrado M, Houry M, Hastings K, Molero-Abraham M, Lozano T, *et al.* PTEN loss confers resistance to anti–PD-1 therapy in non–small cell lung cancer by increasing tumor infiltration of regulatory T cells. Cancer Res 2023; 83:2513-2526.
55. Toyozawa S, Kaminaka C, Furukawa F, Nakamura Y, Matsunaka H, Yamamoto Y. Chemokine receptor CXCR4 is a novel marker for the progression of cutaneous malignant melanomas. Acta Histochem Cytochem 2012; 45:293-299.
56. Mitchell B, Leone D, Feller JK, Bondzie P, Yang S, Park H-Y, *et al.* Correlation of chemokine receptor CXCR4 mRNA in primary cutaneous melanoma with established histopathologic prognosticators and the BRAF status. Melanoma Res 2014; 24:621-625.
57. Longo-Imedio MI, Longo N, Treviño I, Lázaro P, Sánchez-Mateos P. Clinical significance of CXCR3 and CXCR4 expression in primary melanoma. Int J Cancer 2005; 117:861-865.
58. Scala S, Ottaiano A, Ascierto PA, Cavalli M, Simeone E, Giuliano P, *et al.* Expression of CXCR4 predicts poor prognosis in patients with malignant melanoma. Clin Cancer Res 2005; 11:1835-1841.
59. Duda DG, Kozin SV, Kirkpatrick ND, Xu L, Fukumura D, Jain RK. CXCL12 (SDF1α)-CXCR4/CXCR7 pathway inhibition: an emerging sensitizer for anticancer therapies? Clin Cancer Res 2011; 17:2074-2080.
60. André ND, Silva VAO, Watanabe MAE, De Lucca FL. Knockdown of chemokine receptor CXCR4 gene by RNA interference: effects on the B16-F10 melanoma growth. Oncol Rep 2016; 35:2419-2424.
61. D'Alterio C, Buoncervello M, Ieranò C, Napolitano M, Portella L, Rea G, *et al.* Targeting CXCR4 potentiates anti-PD-1 efficacy modifying the tumor microenvironment and inhibiting neoplastic PD-1. J Exp Clin Cancer Res 2019; 38:1-13.
62. Katayama A, Ogino T, Bandoh N, Nonaka S, Harabuchi Y. Expression of CXCR4 and its down-regulation by IFN-γ in head and neck squamous cell carcinoma. Clin Cancer Res 2005; 11:2937-2946.
63. Semmler ML, Bekeschus S, Schäfer M, Bernhardt T, Fischer T, Witzke K, *et al.* Molecular mechanisms of the efficacy of cold atmospheric pressure plasma (CAP) in cancer treatment. Cancers 2020; 12:269.